

Development of Transient Earth Voltage Sensor for Partial Discharge Detection in Gas-insulated Switchgear

Cheng-Chien Kuo,¹ Yu-Ming Liu,¹ and Hung-Cheng Chen^{2*}

¹Department of Electrical Engineering, National Taiwan University of Science and Technology, Taipei 106335, Taiwan

²Department of Electrical Engineering, National Chin-Yi University of Technology, Taichung 411030, Taiwan

(Received July 15, 2023; accepted October 5, 2023)

Keywords: gas-insulated switchgear, transient earth voltage, sensor, partial discharge

The gas-insulated switchgear (GIS) is increasingly used in power systems because of its small size and high reliability. The most common problem in using GIS is partial discharge. To prevent it, insulation is required along with early detection in GIS. The defects inside the GIS need to be found in time to prevent major accidents due to partial discharge. Therefore, we studied the partial discharge detection of GIS to ensure the safety and reliability of GIS operation. Detecting partial discharge also helps to inspect and repair GIS appropriately. In this study, the excitation, transmission, and leakage of electromagnetic waves excited by GIS partial discharge were analyzed as the partial discharge signal of ultrahigh frequency is propagated, reflected, and refracted in GIS by earthing through the outer surface of the metal casing and generating a transient earth voltage. We designed a transient earth voltage sensor on the basis of the characteristics and requirements of GIS. The sensor is used to find defective GIS in operation. The results of the detection of the partial discharge and the signal measurement of defective GIS are important references for online inspection and monitoring.

1. Introduction

Power supply systems are being developed to provide high voltage and large capacity in a small size but with good safety and reliability. The gas-insulated switchgear (GIS) is a substation contained in a closed metal box that is filled with sulfur hexafluoride (SF₆) gas of 0.4–0.5 MPa as a wire conductor to have reliable insulation. According to the CIGRE23.10 survey report,⁽¹⁾ before 1985, 60% of GIS failures were caused by insulation failure. Internal defects of GIS insulation are mainly responsible for accidents and economic losses, and even casualties.⁽²⁾ Insulation failure induces the partial discharge of GIS and affects the condition of the load switch. Partial discharge is found when GIS insulation has defects. Therefore, detecting partial discharge is the best method to assess the condition of the load switch.⁽³⁾

When partial discharge occurs in high-voltage electrical equipment, the discharged electricity is gathered in the metal parts adjacent to the grounding rod, forming a ground current on the

*Corresponding author: e-mail: hcchen@ncut.edu.tw
<https://doi.org/10.18494/SAM4596>

metal surface of the equipment. Internal discharge occurs on the inner surface of the grounding rod but cannot be detected outside the equipment owing to the insulation of the gasket connection, cable insulation terminal, and casing. The high-frequency signal of partial discharge is transmitted to the equipment casing. Therefore, the electromagnetic wave generated by partial discharge is transmitted through the metal case or the liner of GIS and propagates along the outer surface of the case. This generates a transient voltage in the grounding rod. This phenomenon was discovered by Reeves and was named transient earth voltage (TEV).^(4,5)

Partial discharge does not immediately break down the insulation layer, but gradually destroys it with continuous discharge, which eventually leads to the collapse and breakdown of insulation.^(6–8) The generation of partial discharge is accompanied by various physical and chemical phenomena. Thus, detecting partial discharge allows its complete characterization.^(9–11) In this study, we developed a TEV sensor for better detection of TEV caused by partial discharge.

2. GIS

GIS is a high-voltage-level metal-enclosed switchgear filled with SF₆ insulating gas. As one of the GISs, the pole-mounted load break switch (PMLBS) is a three-phase and three-wire GIS. PMLBS is manufactured with SF₆ gas and sprayed sleeve arc elimination to avoid arcing and insulation damage.⁽⁴⁾ Figure 1 shows the load switch made of stainless steel. Its flat structure is to avoid corrosion by rain and acid. The internal contacts and components are insulated with SF₆. It does not require regular maintenance. However, when the SF₆ gas pressure is not sufficiently high to protect the switch, the operation is stopped to avoid accidents. This allows for long life, high reliability, and weather resistance.

The internal structure is shown in Fig. 2, which presents the line load opening and closing switch. The opening and closing of the load switch are operated by moving the insulating arm on the linking shaft.⁽³⁾ The arc generated during the opening and closing is extinguished by the movable contact and blowing SF₆. Then, the internal insulation is protected from the arc and the deterioration of the insulation is avoided.⁽¹²⁾ Otherwise, the arc affects the insulating ability and the normal operation of the load switch. The load switch contains a porcelain casing, a fixed electrode rod, a connecting shaft, a movable contact, a fixed contact, an insulated operation arm, and a blowing cylinder.



Fig. 1. (Color online) SF₆ line load switch on rod.

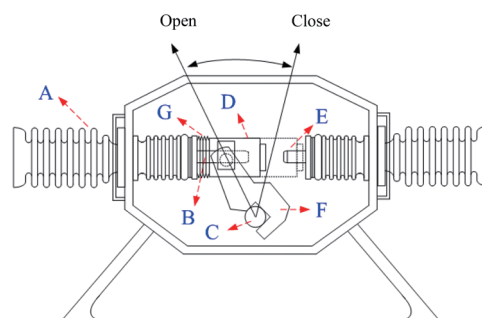


Fig. 2. (Color online) Internal structure of SF₆ line load switch.

3. Internal Defects of GIS

Other than metal particles inside the case of the load switch, defects are also found in the internal switch and mechanical structure, which are not found easily by manual inspection. We used a three-phase 15 kV rod-type SF₆ line load switch in the experiment. Defects are frequently found in the load switch, such as oil stains in the porcelain casing on the load side, metal particles in the case, foreign objects on the connecting shaft, metal protrusions on the ring of the load switch, and metal fatigue on the load and highly pressurized sides. Figure 3 shows a photo of the load switch. Figures 4–7 depict the various defects of the load switch. The analysis of the structure of the single-phase load switch can help to avoid the partial discharge caused by various defects. These defects can be found in each situation caused by a defect.

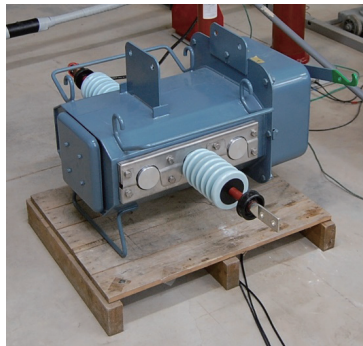


Fig. 3. (Color online) Photo of load switch.

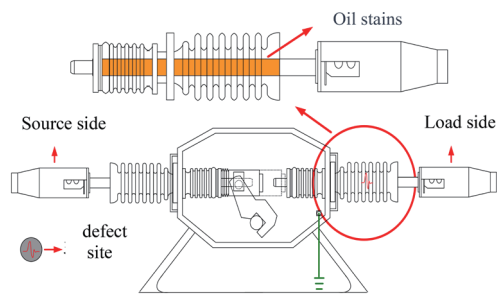


Fig. 4. (Color online) Oil stains in porcelain casing on the load side.

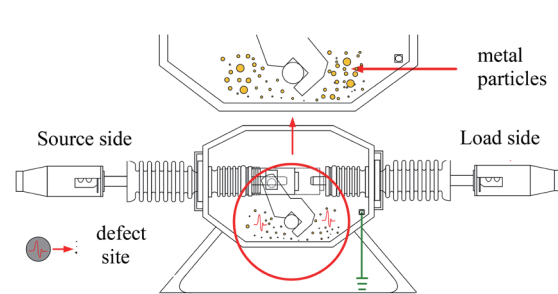


Fig. 5. (Color online) Metal particles in connecting shaft.

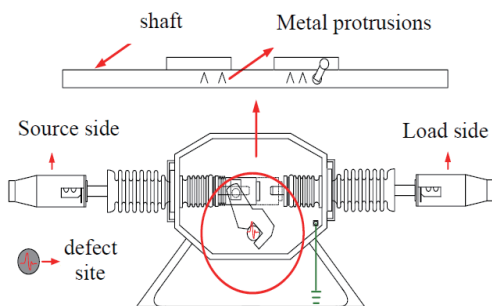


Fig. 6. (Color online) Metal protrusions on connecting shaft.

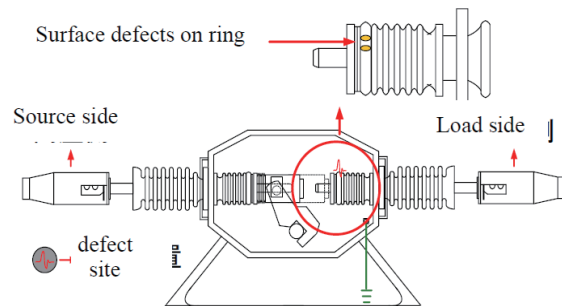


Fig. 7. (Color online) Metal fatigue on load and source sides.

4. Detection Method

The TEV detection method requires a capacitive sensor to detect partial discharge. When the partial discharge is generated, the voltage and current propagate along the metal casing and spread on its surface to be earthed in the gap between the opening and the inside as shown in Fig. 8.⁽¹³⁾ The voltage is only changed from a few millivolts to volts in nanoseconds, so the signal range of TEV is limited.⁽¹⁴⁾

When partial discharge occurs inside the load switch, the discharged current gathers on the internal surface of the metal casing and its signal propagates to the surface. Through gaps at the connection and insulation parts, the TEV is generated on the ground rod as shown in Fig. 9.^(15,16)

According to the principle of TEV generation, the metal casing becomes an electrode, a silicone sheet is an insulating medium, and a copper sheet is a capacitor C_1 . The discharge signal is obtained on both ends of capacitors C_1 and C_2 . From the theory, the larger the surface area of the copper sheet, the larger the value of C_1 , and the better to detect the partial discharge signal (Fig. 10).

$$c = \frac{\epsilon_r \epsilon_0 S}{d} \tag{1}$$

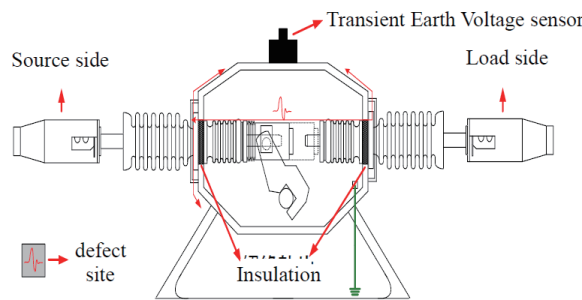


Fig. 8. (Color online) TEV detection method.

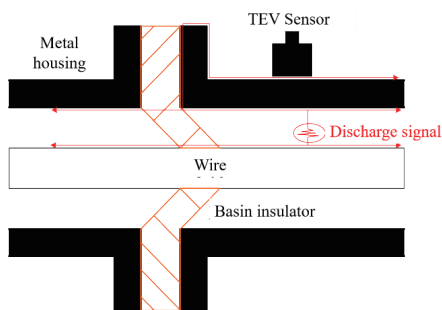


Fig. 9. (Color online) Occurrence of TEV.

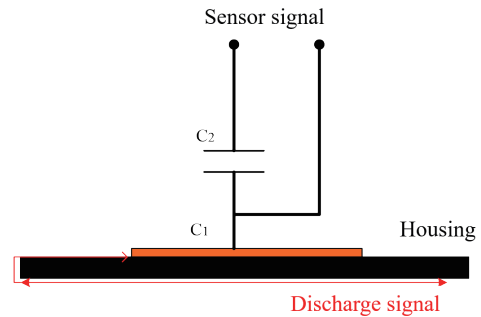


Fig. 10. (Color online) Diagram of TEV sensor.

Here, ϵ_r is the dielectric constant of the silicone film and ϵ_0 is that of the vacuum. The size of GIS is considered assuming that GIS is circular. When the area of the copper sheet is very large, the silicone sheet must have a corresponding area that is impossible.

5. TEV Sensor Design

Figure 11 shows the six different silicone sheets used in this study, which are cut into squares with a side length of 5 cm. The first, second, and third silicone sheets have the same transparent color but with different thicknesses (3, 2, and 1 mm, respectively). The fourth silicone sheet has a dark blue color and a thickness of 2 mm. The fifth silicone sheet has a gray color and a thickness of 1 mm, and the back side is glued to adhere to the surface easily. The sixth silicone sheet has a blue color and a thickness of 0.3 mm.

The dielectric constants of the silicone sheets are measured by placing a square of the sheet with a side length of 5 cm in the middle of two thin copper square sheets of the same size to form a capacitor. The copper sheet is shown in Fig. 12.

To make the copper sheet fit to the silicone sheet and not have gaps between the sheets, tape is used to ensure that there are no air gaps in the middle. Then, the HIOKI_IM3523 LCR METER is used to measure capacitance as shown in Fig. 13. The dielectric constant of the silicone sheet was calculated by the method described in Ref. 1, and the results are shown in Table 1.

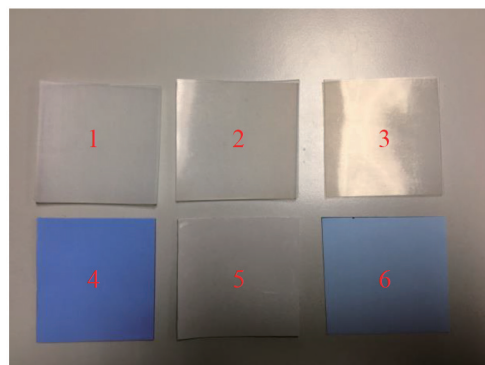


Fig. 11. (Color online) Different silicone sheets used in this study.



Fig. 12. (Color online) Copper sheet.

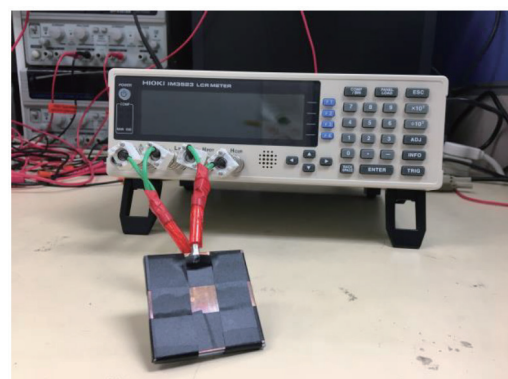


Fig. 13. (Color online) Measurement of capacitance.

Table 1
Specifications and dielectric constants of silicone sheets.

Silicone sheet	Thickness (mm)	Dielectric constant
1	3	3.278492099
2	2	3.046925508
3	1	2.67468716
4	2	4.490455982
5	1	3.008848758
6	0.3	1.4668307

After obtaining the dielectric constants of the silicone sheets, the capacitance C_1 was calculated and the capacitance C_2 was selected. The original amplifier signal was projected back after measuring the signal. The first, fifth, and sixth silicone sheets were very thin, so it was impossible to make them stick to the metal casing, whereas the fourth silicone sheet was soft and its ductility was not good so it could easily be cracked and damaged.

The TEV sensor shell was made of aluminum, which can shield the external interference signal. The TEV sensor casing was made of aluminum ($50 \times 45 \times 30 \text{ mm}^3$) as shown in Fig. 14. The sensor did not have direct contact with the metal housing of the load switch to avoid a leakage of current when the metal housing had a leakage current. The BNC connector was inserted and fixed on the sensor. C_1 and C_2 were connected in series and fixed inside the aluminum box, and then the silicone sheet was glued on. The diagram of the TEV sensor is shown in Fig. 15.

To verify the operation of the TEV sensor, we used it for silicone sheets of different thicknesses and high-frequency current converters (HFCTs) to detect the partial discharge for comparison. Figure 16 shows the results of the TEV and HFCT sensors for the second silicone sheet of 2 mm thickness. The yellow line is for the applied voltage signal, the red line is for the HFCT detection signal, and the blue line is for the TEV sensor detection signal. Although the discharge signal was detected at the same time point, the frequency of the signal detected by the TEV sensor was about 30 times higher than that detected by the HFCT sensor. The bandwidth of the TEV sensor was higher than that of the HFCT sensor, whereas the amplitude of the HFCT sensor was higher than that of the TEV sensor.

Figure 17 shows the measurement results of discharge with the TEV and HFCT sensors for the silicone sheet of 3 mm thickness. The oscillation frequency of the signal detected by the TEV sensor was higher than that detected by the HFCT sensor. The detection time of the TEV sensor was shorter than that of the HFCT sensor as the latter was used as an inductive sensor, and thus, its inductance took a longer time. The amplitude of the signal detected by the HFCT sensor was higher than that detected by the TEV sensor. The reason was that the propagation direction of the partial discharge was random, which led to energy loss and differences in TEV. In applications, the TEV sensor can be installed more easily than the HFCT sensor.

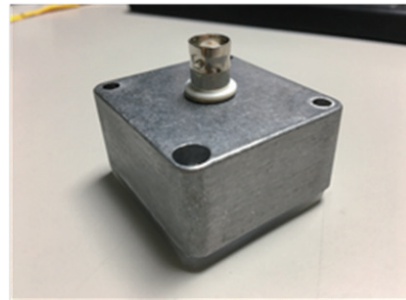
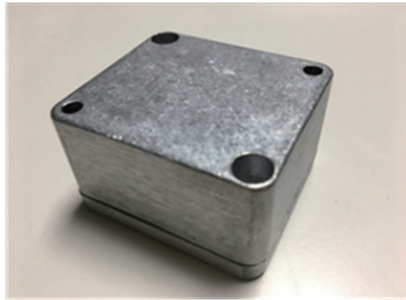


Fig. 14. (Color online) Aluminum housing of TEV sensor.

Fig. 15. (Color online) Photo of TEV sensor.

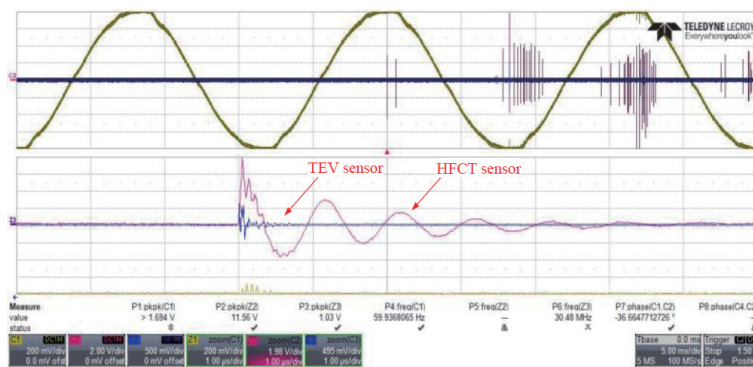


Fig. 16. (Color online) Measurement results of discharge with TEV and HFCT sensors for silicone sheet of 2 mm thickness.

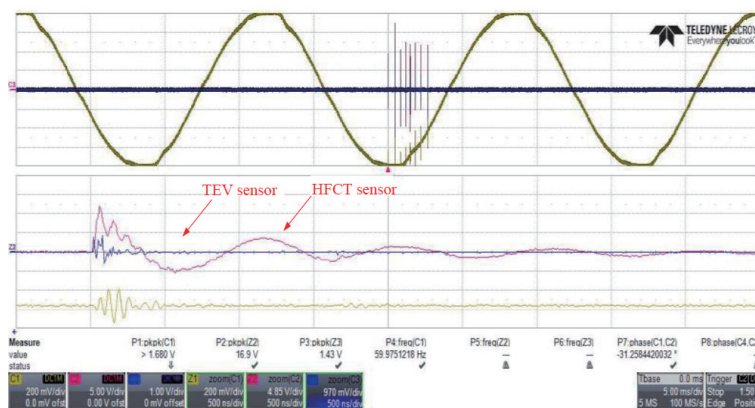


Fig. 17. (Color online) Measurement results of discharge with TEV and HFCT sensors for silicone sheet of 3 mm thickness.

6. Test Results and Discussion

6.1. Procedure

In addition to the normal operation of the TEV sensor, the detection of the partial discharge must satisfy the criteria before the installation and operation of the load switch. To stabilize the data collection and increase the credibility of the results, the tests were conducted according to

the standard operation. Figure 18 shows the standard load switch test procedure IEC 60044-2-2003 and TPC C039 specification, as well as the test conditions and test flow diagram of this study.

6.2. GIS detection platform

To simulate the discharge caused by GIS faults, an offline test was conducted. In the simulation, special care must be taken and a certain distance must be kept from the oscilloscope, so a relatively long cable was used. The TEV sensor was fixed with electrical tape to make the gap between the sensor and the GIS casing smaller and increase the accuracy of the sensor because the sensor needed to be in close contact with the GIS metal casing (Figs. 19 and 20).

6.3 Results

The partial discharge was measured in the complete partial discharge waveform as shown in Fig. 21. The oscillation caused by the TEV sensor after detecting the discharge signal is the inductive nature of the transmission line showing the high frequency of the signal. Figure 22 shows that the best signal among the separated three signals was measured by the TEV sensor with a silicone sheet of 2 mm thickness.

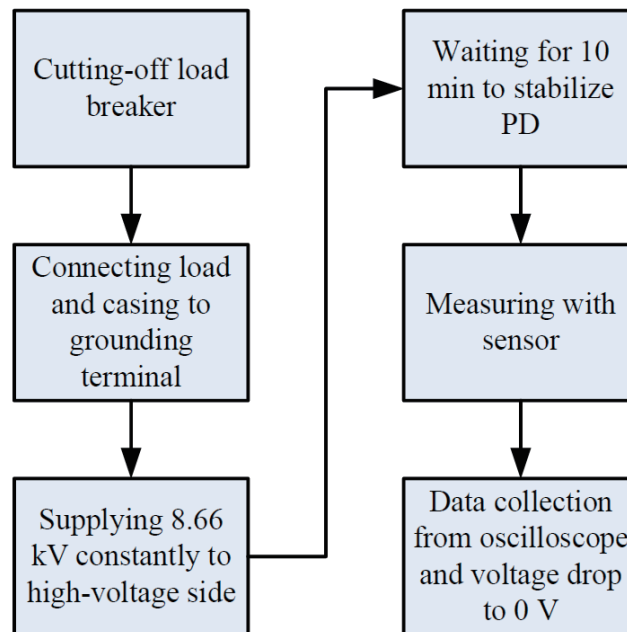


Fig. 18. (Color online) Test procedure.

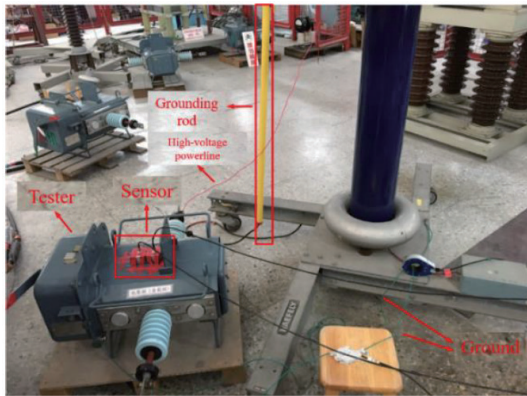


Fig. 19. (Color online) Off-line test platform.

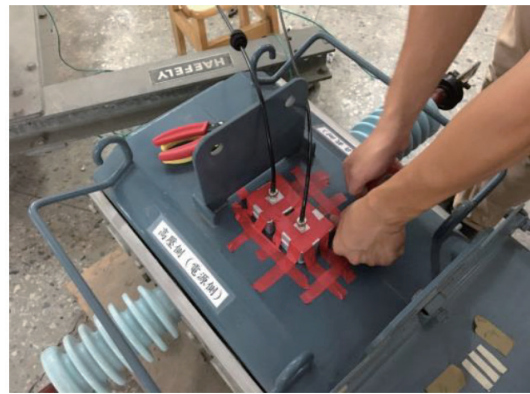


Fig. 20. (Color online) TEV sensor fixed on GIS.

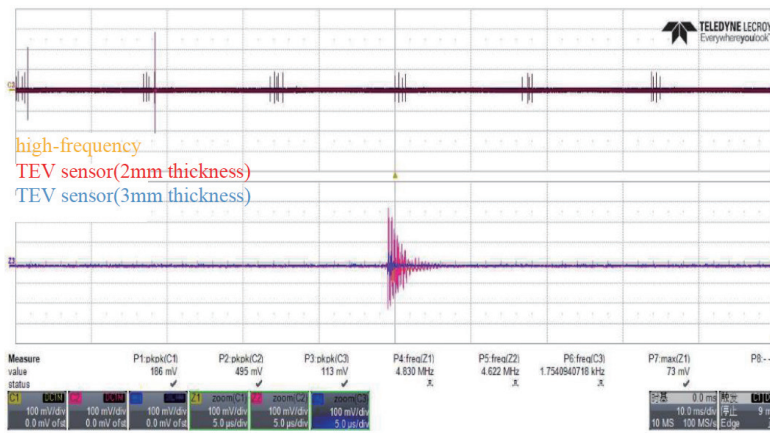


Fig. 21. (Color online) TEV sensor detection results.

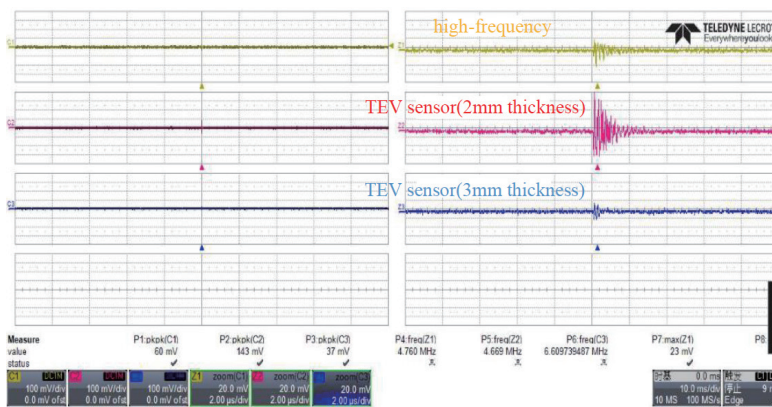


Fig. 22. (Color online) Test result of TEV sensor.

7. Conclusion

In maintaining the SF₆ load switch, human errors are inevitably caused during the detection of the defects of the equipment, which may lead to the poor power quality of the high-voltage supply and unexpected incidents. TEV is generated by the electromagnetic wave of the partial discharge of GIS and propagates to the ground rod through the gap along the metal casing. Thus, we designed and developed a TEV sensor that could be used for the partial discharge detection of load switches. The detection of TEV becomes efficient and easy with the TEV sensor, and the inspection of GIS can be performed at a lower cost as a large number of sensors can be deployed to detect partial discharge signals. In the future, the TEV sensor can be combined with chaos synchronization to investigate the signal characteristics and build a GIS fault diagnosis system with extension theory.

References

- 1 R. Nanarsheth and S. Singh: *J. Electr. Power Energy Syst.* **55** (2014) 481. <https://dx.doi.org/10.1016/j.ijepes.2013.09.012>
- 2 X. Zhang, F. Meng, and B. Yang: *IEEE Trans. Dielectr. Electr. Insul.* **20** (2013) 2246. <https://doi.org/10.1109/TDEI.2013.6678876>
- 3 C.-M. Hwang, J.-O. Choi, C.-K. Choi, and I.-S. Jung: *Proc. 2008 IEEE Int. Symp. Electrical Insulation (IEEE, 2008)* 400–403. <https://doi.org/10.1109/ELINSL.2008.4570358>
- 4 N. Davies, Y. Tian, J. Cheung, Y. Tang, and P. Shiel: *Proc. 2008 Int. Conf. Condition Monitoring and Diagnosis (IEEE 2008)* 385. <https://doi.org/10.1109/CMD.2008.4580307>
- 5 G. Dennis, M. Redfern, and S. Pennock: *Proc. 2006 Int. Universities Power Engineering Conf. (IEEE, 2006)* 814. <https://doi.org/10.1109/UPEC.2006.367593>
- 6 S. Kaneko, S. Okabe, H. Muto, M. Yoshimura, C. Nishida, and M. Kamei: *IEEE Trans. Dielectr. Electr. Insul.* **16** (2009) 60. <https://doi.org/10.1109/TDEI.2009.4784552>
- 7 S. Kaneko, S. Okabe, M. Yoshimura, H. Muto, C. Nishida, and M. Kamei: *IEEE Trans. Dielectr. Electr. Insul.* **16** (2009) 1462. <https://ieeexplore.ieee.org/document/5293961>
- 8 I. J. Kemp: *IEEE Proc. Sci. Meas. Technol.* **142** (1995) 4. <https://doi.org/10.1049/IP-SMT%3A19951438>
- 9 M. D. Judd, O. Farish, and B. F. Hampton: *IEEE Proc. Sci. Meas. Technol.* **142** (1995) 237. <https://doi.org/10.1049/ip-smt:19951699>
- 10 L.-J. Jin, J.-Q. Huang, W.-D. Liu, and J.-L. Qin: *Proc. 2001 Int. Symp. Electrical Insulating Materials (ISEIM, 2001)* 137. <https://doi.org/10.1109/ISEIM.2001.973636>
- 11 M. D. Judd and O. F. P. F. Coventry: *IEEE Sci. Meas.* **144** (1997) 117. <http://doi.org/10.1049/ip-smt:19971130>
- 12 M. Hikita, H. Yamashita, and T. Katod: *Proc. 1994 Int. Conf. Properties and Applications of Dielectric Material (IEEE, 1994)* 570. <https://doi.org/10.1109/ICPADM.1994.414074>
- 13 E. Jennings and A. Collinson: *IEEE 1993 Int. Conf. Partial Discharge (IEEE, 1993)* 28.
- 14 L.-H. Wang, H.-J. Wang, L.-J. Wang, H. Lu, W.-J. Ning, S.-L. Jia, and J. Wu: *Proc. 2013 IEEE 4th Int. Conf. Electric Power Equipment—Switching Technology (IEEE, 2013)* 1. <https://doi.org/10.1109/ICEPE-ST.2013.6804296>
- 15 T. Han, B.-X. Du, Y. Gao, and Y.-S. Xia: *Proc. 2012 IEEE Int. Conf. Innovative Smart Grid Technologies—Asia (IEEE, 2012)* 1. <https://doi.org/10.1109/ISGT-Asia.2012.6303173>
- 16 Y. W. Li, Y.-Y. Wang, G.-J. Lu, J. Wang, and J. Xiong: *Proc. 2010 Int. Conf. High Voltage Engineering and Application (IEEE, 2010)* 309. <https://doi.org/10.1109/ICHVE.2010.5640801>